

A multi-wavelength study of the proto-cluster surrounding the $z=4.1$ radio galaxy TN J1338–1942.*

Carlos De Breuck^{1,2}, Frank Bertoldi³, Chris Carilli⁴, Alain Omont², Bram Venemans⁵, Huub Röttgering⁵,
Roderik Overzier⁵, Michiel Reuland^{5,6,7}, George Miley⁵, Rob Ivison⁸, and Wil van Breugel⁶

¹ European Southern Observatory, Karl Schwarzschild Straße 2, D-85748 Garching, Germany
e-mail: cdebreuc@eso.org

² Institut d'Astrophysique de Paris, CNRS, 98bis Boulevard Arago, F-75014 Paris, France
e-mail: omont@iap.fr

³ Max Planck Institut für Radioastronomie, Auf dem Hügel 69, D-53121 Bonn, Germany
e-mail: bertoldi@mpifr-bonn.mpg.de

⁴ National Radio Astronomy Observatory, P.O. Box O, Socorro, NM 87801, USA
e-mail: ccarilli@nrao.edu

⁵ Sterrewacht Leiden, Postbus 9513, NL-2300 RA Leiden, The Netherlands
e-mail: rottgeri,venemans,overzier,miley@strw.leidenuniv.nl

⁶ IGPP/LLNL, L-413, 7000 East Ave, Livermore, CA 94550, USA
e-mail: mreuland,wil@igpp.ucllnl.org

⁷ Department of Physics, University of California, Davis, CA 95616, USA

⁸ Institute for Astronomy, University of Edinburgh, Royal Observatory, Blackford Hill, Edinburgh EH9 3HJ,
United Kingdom
e-mail: rji@roe.ac.uk

Received 2003 December 16; accepted 2004 May 14

Abstract. We present a 1.2 mm (250 GHz) map obtained with MAMBO on the IRAM 30m telescope of the central 25 arcmin² of the proto-cluster surrounding the $z=4.1$ radio galaxy TN J1338–1942. The map reaches a 1σ sensitivity of 0.6 mJy in the central area, increasing to 1.2 mJy at the edges. We detect 10 candidate mm sources, of which 8 are also detected in a deep VLA 1.4 GHz map and/or a VLT R -band image. Three sources have a flux density $S_{1.2\text{mm}} > 4.0$ mJy, representing a 7σ overdensity compared to random field surveys, which predict only 1 such source in our map area. We obtained SCUBA/JCMT 850 μm and 450 μm photometry of six radio/optically identified MAMBO sources, confirming 5 of them with $S/N > 4$. Radio-to-mm and mm-to-submm redshift estimators cannot put strong constraints on the redshifts of these MAMBO sources, but 9 of them are consistent within the uncertainties (mean $\Delta z = +2.6$) with $z=4.1$. One faint MAMBO source is possibly identified with an extremely red object ($R - K = 6.1$) at a likely spectroscopic redshift $z=1.18$.

The four brightest MAMBO sources are all located north of the radio galaxy, while the densest area of companion Ly α excess and Lyman break galaxies is to the southeast. None of the 14 spectroscopically confirmed Ly α emitters in the MAMBO field are detected at 1.2 mm; their average 1.2 mm flux density is $\langle S_{1.2\text{mm}} \rangle = 0.25 \pm 0.24$ mJy. If the mm sources lie at $z=4.1$, none of them show excess Ly α emission in our narrow-band images. Both populations thus show no apparent overlap, possibly due to dust quenching the Ly α emission. If the mm sources are part of the proto-cluster, our results suggest that galaxies with star formation rates of a few $1000 \text{ M}_{\odot} \text{yr}^{-1}$ could be spread throughout the proto-cluster over projected scales of at least 2 Mpc.

Key words. Galaxies: individual: TN J1338-1942 – galaxies: clusters: individual: TN J1338-1942 – galaxies: formation – cosmology: observations

Send offprint requests to: Carlos De Breuck

* Based on observations obtained with the IRAM 30m, the Very Large Array, the James Clerk Maxwell Telescope, and the ESO Very Large Telescope at Paranal, Chile (programs LP167.A-0409, 69.B-0078 and 71.A-0495).

1. Introduction

Our knowledge of large-scale structures at high redshifts has made significant progress in recent years with the detection of several overdense regions out to

$z > 4$ (*e.g.* Steidel et al., 1998; Pentericci et al., 2000; Venemans et al., 2002; Shimasaku et al., 2003). The discovery of these proto-clusters with sizes of several Mpc was made possible by deep wide-field optical surveys, concentrating on a narrow redshift interval using the Lyman-break or narrow-band Ly α (Kurk et al., 2000; Venemans et al., 2002) or H α (Kurk et al., 2004) excess techniques, followed by multi-slit spectroscopy on 8-10m telescopes. Similar surveys have also been done in random fields (*e.g.* Hu et al., 1998, 2002; Rhoads et al., 2003; Kodaira et al., 2003; Shimasaku et al., 2003).

Hierarchical galaxy formation models (*e.g.* Kauffmann et al., 1999) predict that the best fields to search for such overdensities are those containing a massive galaxy. High redshift radio galaxies (HzRGs; $z > 2$) are therefore ideal targets, as they are not only among the most massive galaxies known at high z (*e.g.* De Breuck et al., 2002; Rocca-Volmerange et al., 2004), but their lower redshift ($z \gtrsim 0.5$) counterparts are also located in cluster environments (*e.g.* Hill & Lilly, 1991; Best, 2000; Best et al., 2003). This motivated an intensive search of Ly α emitting companions around six radio galaxies with $2.1 < z < 4.1$, leading to the discovery of overdensities of Ly α emitters of 5 to 15 compared with the random fields (Venemans et al., 2002, 2003).

However, the Ly α excess technique detects only a fraction of the companion objects. For example, in the proto-cluster of Lyman break galaxies at $z=3.09$ in the SSA 22 region (LBG; Steidel et al., 1998), only 25% of the LBGs have a sufficiently high Ly α equivalent width to be included in a Ly α excess selection (Steidel et al., 2000). This incompleteness is also illustrated by the presence of a similar overdensity of H α emitters and extremely red objects in the proto-cluster surrounding the $z=2.16$ radio galaxy PKS 1138–262, while these galaxies are mostly not detected using the Ly α excess technique (Kurk et al., 2004). Deep *Chandra* observations of this field have also found an overdensity of X-ray sources, of which at least 2 are AGN within the proto-cluster (Pentericci et al., 2002). Smail et al. (2003b) also report the detection of four *Chandra* X-ray sources coincident with submm sources surrounding three HzRGs.

These proto-clusters also contain a large amount of gas, as revealed by the Ly α haloes surrounding the HzRGs, which have physical scales up to >200 kpc (for a recent review, see van Breugel et al., 2003). Together with the increased merger rates in higher redshift clusters (*e.g.* van Dokkum et al., 1999), this provides the ingredients to induce wide-spread starbursts and AGN, which could be revealed by their thermal dust (sub-)mm emission. Statistical overdensities of (sub-)mm galaxies (SMGs) have indeed been found from SCUBA bolometer imaging of the fields surrounding the $z=3.09$ 'redshift spike' (Chapman et al., 2001), the $z=2.39$ radio galaxy 53W002 (Smail et al., 2003a), the $z=3.8$ radio galaxy 4C 41.17 (Ivison et al., 2000), a $z=1.8$ QSO (Stevens et al., 2004) and six other HzRG fields (Stevens et al., 2003). In this paper, we present a 1.2 mm map covering the

central 25 arcmin^2 of the most distant proto-cluster known to date, surrounding the $z=4.1$ radio galaxy TN J1338–1942. We find an overdensity of 1.2 mm sources, which we identify with optically very faint galaxies using a deep 1.4 GHz map, but find no overlap between the population of excess Ly α emitters and the 1.2 mm sources. Throughout this paper, we use a Λ -cosmology with $H_0=71 \text{ km s}^{-1} \text{ Mpc}^{-1}$, $\Omega_M=0.27$ and $\Omega_\Lambda=0.73$ (Spergel et al., 2003; Tonry et al., 2003). At $z=4.1$, the luminosity distance is $D_L=37.65 \text{ Gpc}$, and $1''$ corresponds to 7.0 kpc.

2. Observations and data reduction

2.1. IRAM 1.2mm imaging

To image the field of TN J1338–1942 at mm wavelengths, we used the 37- and 117-channel Max Planck Bolometer arrays (MAMBO-1 and MAMBO-2; Kreysa et al., 1998) at the IRAM 30m telescope on Pico Veleta, Spain. MAMBO has a half-power spectral bandwidth from 210 to 290 GHz, with an effective bandwidth centre for steep thermal spectra of $\sim 250 \text{ GHz}$ (1.2 mm). The effective beam FWHM is $10''.7$ with an array size of $4'$.

The observations were done in a pooled observing mode during the winter 2001-2002 season. Due to the low declination, the field could only be observed for 4 hours in a given night, with elevations between 29° and 33° . The atmospheric zenith opacities at 1.2 mm varied between 0.12 and 0.25. The total on source integration time was 17.0 hours, of which 2.6 h were obtained with the 117-channel array, and 14.6 h with the 37-channel array. We used the standard on-the-fly mapping technique, comprised of 41 subscans of 40 s each, while chopping the secondary mirror in azimuth at 2 Hz. To minimize the residual effects of the double beam point spread function, we used different chop (wobbler) throws ($39''$, $42''$ or $45''$) and/or scan directions for each map. We used 7 different pointings offset by $80''$ to cover the entire field of the VLT/FORS2 imaging to uniform depth. We checked the pointing and focus at least once per hour using the bright point source 1334–127, and found the pointing to be stable to within $<2''$. The absolute flux calibration is based on observations of several standard calibration sources, including planets, resulting in an estimated accuracy of 15%.

We analyzed the data using the MOPSI software package (Zylka, 1998). We subtracted the skynoise, and combined the double-beam maps using a shift-and-add procedure, producing for each map a positive image bracketed by two negative images of half the intensity located one chop throw away. Because we combined our 37 maps obtained with different chop throws, the effect of the confusion due to negative sidelobes is minimized, but still present in regions of high source density. The noise level increases outward in our co-added map of the field. In Fig. 1 two contours show the region within which the rms noise level is less than 1.2 and 0.6 mJy (before smoothing), enclosing areas of 25.6 and 2.6 square arcmin, respectively.

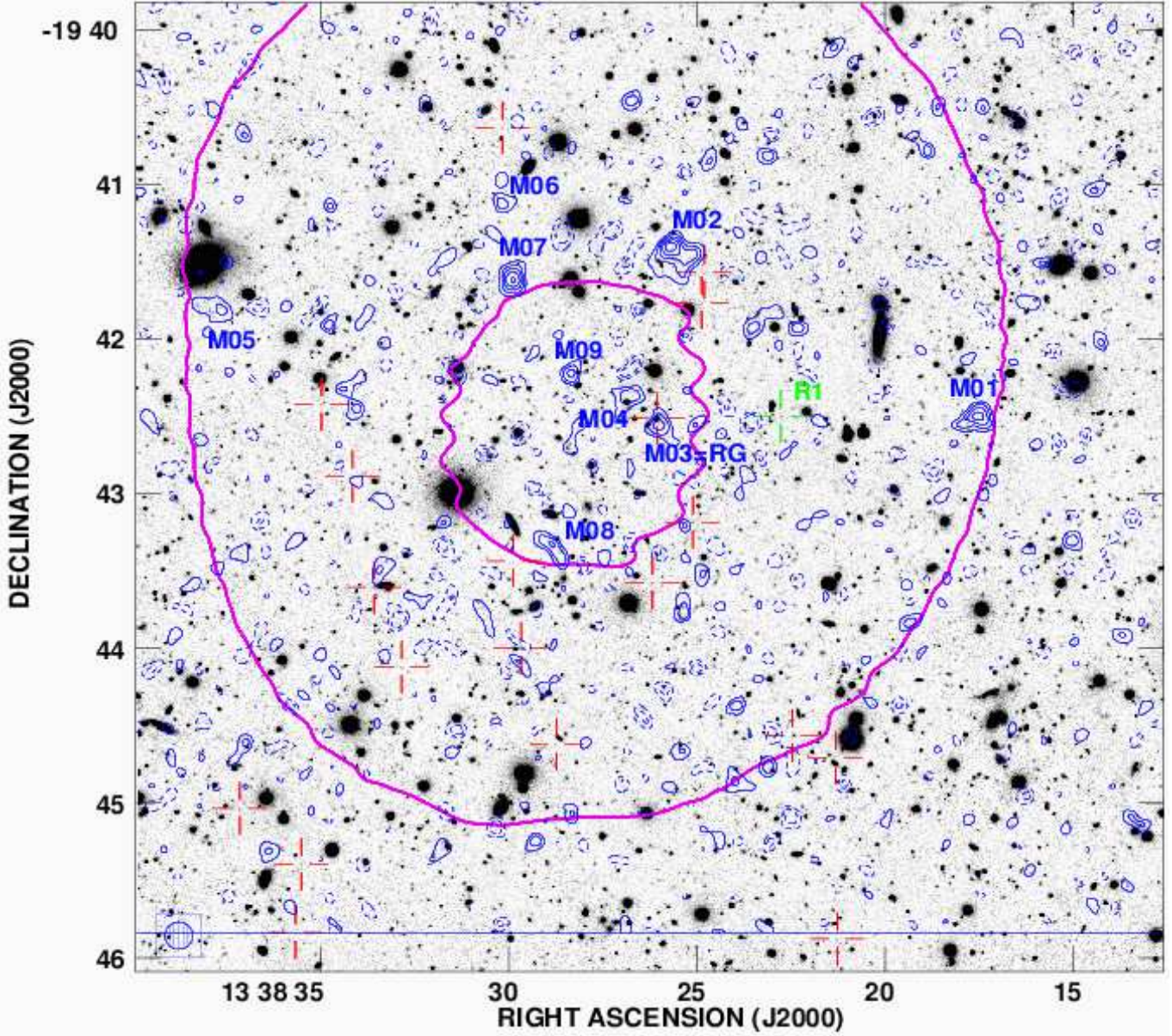


Fig. 1. VLT R -band image (greyscale; Venemans et al., 2002) with MAMBO 1.2 mm signal-to-noise map (smoothed to $11''$) overlaid as thin/blue contours. Contour levels are -3 , -2 , 2 , 3 , 4 and 5σ , with σ the local rms noise level (negative contours are dashed). The two large purple contours delineate the regions with $\sigma < 0.6$ and 1.2 mJy/beam. The MAMBO beam size is indicated in the lower left corner. The red open crosses indicate spectroscopically confirmed $\text{Ly}\alpha$ companions to the radio galaxy TN J1338–1942, and the green open cross labeled R1 an additional FR II radio source.

2.2. VLA radio imaging

To obtain accurate positions of the mm sources, and to search for possible radio-loud AGN counterparts, we observed the TN J1338–1942 field with the Very Large Array (VLA; Napier, Thompson & Ekers, 1983) on UT 2002 April 1 to 12 for a total of 12 hours in the A-array at 20 cm. We observed in a pseudo-continuum, spectral line mode with 7×3.125 MHz channels. We monitored the point source 1351–148 every 40 min to provide amplitude, phase and bandpass calibration, and used an observation of 3C 286 to provide the absolute flux calibration.

We performed standard spectral-line calibration and editing of the data using the NRAO *AIPS* package, and employed standard wide field imaging techniques (Taylor, Carilli, & Perley, 1999). The final 7.5×7.5 image has an rms noise level of $15 \mu\text{Jy beam}^{-1}$, except in the area close to the central radio galaxy, which is limited by the ability to clean the bright radio source (see Fig. 2). The FWHM resolution of the restoring beam is $2''.3 \times 1''.3$ at a position angle $\text{PA}=0^\circ$.

Table 1. Astrometry of the MAMBO, VLA and VLT sources in the TN J1338–1942 field.

Source	MAMBO		VLA		VLT	
	RA(J2000) <i>h m s</i>	DEC(J2000) <i>° ′ ″</i>	RA(J2000) <i>h m s</i>	DEC(J2000) <i>° ′ ″</i>	RA(J2000) <i>h m s</i>	DEC(J2000) <i>° ′ ″</i>
M01	13 38 17.56	−19 42 30.7	13 38 17.48	−19 42 29.5	13 38 17.43	−19 42 29.9
M02a	13 38 25.65	−19 41 25.5	13 38 25.47	−19 41 21.5	13 38 25.45	−19 41 22.1
M02b			13 38 25.37	−19 41 26.5		
M02c			13 38 25.81	−19 41 26.2		
M03	13 38 25.97	−19 42 33.9	13 38 26.10	−19 42 31.3	13 38 26.06	−19 42 30.7
M04	13 38 26.84	−19 42 22.8	13 38 26.83	−19 42 25.8	13 38 26.82	−19 42 26.2
M05	13 38 37.79	−19 41 48.8	13 38 37.91	−19 41 49.1	13 38 37.92	−19 41 48.9
M06	13 38 30.13	−19 41 06.5	13 38 30.04	−19 41 04.5	13 38 30.06	−19 41 04.7
M07	13 38 29.89	−19 41 36.9
M08	13 38 28.86	−19 43 20.9	13 38 28.77	−19 43 27.5
M09	13 38 28.33	−19 42 13.2
M10	13 38 29.78	−19 39 32.1	13 38 29.81	−19 39 31.9	... ^a	... ^a
R1	13 38 22.77	−19 42 30.0	13 38 22.76	−19 42 29.9

^a This source is located outside the VLT image boundary.**Table 2.** Photometry of the MAMBO and VLA sources in the TN J1338–1942 field.

Source	$S_{20\text{cm}}$ μJy	$S_{1200\mu\text{m}}$ mJy/beam	$S_{850\mu\text{m}}$ mJy	$S_{450\mu\text{m}}$ mJy	$R[3'']$ mag	$NB[3'']$ mag	$K[3'']$ mag
M01	148±34	6.2±1.2	10.1±1.3	21.5±6.4	26.8±0.3	>28	... ^a
M02a	54±25	4.1±0.8	6.6±1.3^b	12.5±6.0 ^b	25.6±0.1	26.7±0.7	... ^a
M02b	46±25				>28	>28	... ^a
M02c	47±26				>28	>28	... ^a
M03	120800±4300	2.3±0.6	6.1±1.3^c	25.3±9.3	22.38±0.01	19.2±0.1	19.97±0.05
M04	47±17	2.0±0.5	24.08±0.03	24.9±0.2	18.72±0.03
M05	91±25	3.8±0.8	9.9±1.2^b	14.9±5.9 ^b	25.06±0.07	25.6±0.3	... ^a
M06	41±24	2.3±0.6	5.7±1.3	<20 (3 σ)	27.8±0.8	>28	... ^a
M07	<50 (3 σ)	4.0±0.6	3.3±2.0	<33 (3 σ)	>28	>28	... ^a
M08	<50 (3 σ)	2.4±0.7	25.26±0.09	26.0±0.4	19.2±0.1
M09	<50 (3 σ)	2.3±0.6 ^d	... ^d	... ^a
M10	195±28	3.2±1.0 ^a	... ^a	... ^a
R1	10900±400	<1.8 (3 σ)	25.6±0.1	25.6±0.3	... ^a

^a Source located outside the coverage of the VLT/Keck images.^b SCUBA flux densities could be underestimated due to the extent of the 1.2mm source (see §3.2 and Fig. 3).^c We quote the S/N weighted average of our value ($S_{850\mu\text{m}} = 3.1 \pm 1.8$) and the value quoted by Reuland et al. (2004) ($S_{850\mu\text{m}} = 6.9 \pm 1.1$).^d No clear optical/near-IR counterpart.

2.3. JCMT submm photometry

We obtained 850 μm and 450 μm photometry of 6 MAMBO sources previously identified using the VLA and VLT imaging (§3.1) using the Submillimetre Common-User Bolometer Array (SCUBA; Holland et al., 1999) on the 15m James Clerk Maxwell Telescope on UT 2003 February 17 to 22, for a total integration time of 16 hours (including overheads) spread over 6 sources. The respective beamsizes are $14''.7$ at 850 μm and $7''.5$ at 450 μm . We used the recommended 9-point jiggle photometry mode, which samples a 3×3 grid with $2''$ spacing between grid points, while chopping in azimuth by $60''$. The atmospheric conditions were excellent, with zenith opacities at 850 μm varying between 0.11 and 0.24. We checked the pointing and focus roughly once per hour using the bright point source 1334–127, and found the pointing to be sta-

ble within $<3''$. The absolute flux calibration is based on observations of CRL618 and Mars.

We reduced the data in the standard way using SCUBA User Reduction Facility (SURF; Jenness, 1997). We removed individual data samples that were deviant from the mean by $>4\sigma$ from the data set, flatfielded, corrected for extinction, despiked, and subtracted the residual sky level from the off-source bolometers. Finally, we calculated the mean and rms from the time sequence to remove all points deviating by more than 3σ from the mean. We adopt the mean of the remaining data as our final estimate of the intensity.

2.4. Optical and near-IR imaging and spectroscopy

Optical and near-IR imaging data of the TN J1338–1942 field exist in the literature. De Breuck et al. (1999) pub-

lished a NIRC/Keck K -band image covering the central $1' \times 1'$, centred on the radio galaxy. Venemans et al. (2002) published deep R -band and narrow-band Ly α images obtained with the FOCAL Reducer/low dispersion Spectrograph (FORS) at the ESO Very Large Telescope (VLT), covering $6'.4 \times 6'.2$, and also spectroscopically confirmed 20 Ly α emitters in this field, of which 15 fall within the $\sigma < 1.2$ mJy region of our MAMBO map. Overzier et al. (in prep.) also obtained a K -band image of the south-eastern corner of the proto-cluster with the Infrared Spectrometer And Array Camera (ISAAC) at the VLT. In the following, we shall use both the K -band and R -band images to identify the optical counterparts of the mm and radio sources. We corrected all magnitudes for Galactic extinction $E(B - V) = 0.097$ using the dust maps of Schlegel, Finkbeiner, & Davis (1998) and the extinction curve of Cardelli, Clayton, & Mathis (1989).

Optical spectroscopy of three sources (M01, M05 and M08) was obtained as part of two VLT multi-slit spectroscopy programs. Details about these observations will be given in future papers (De Breuck et al., in preparation; Overzier et al., in preparation).

3. Results

3.1. Extraction of the mm sources

We use the MAMBO signal-to-noise map (Fig. 1) to identify candidate mm sources within the region where $\sigma < 1.2$ mJy/beam. To assess the reliability of the candidate sources, we also made 'probability maps' by splitting up the data sets, and looking for gross discrepancies between them. This would identify spurious sources appearing in only part of the data. The reliability of our positive detections is further strengthened by the absence of negative peaks $< -4\sigma$ in the S/N map (dashed contours in Fig. 1). The three most significant negative sources are all located in between M02 and M07, consistent with them being residual double beaming effects (see §2.1).

Table 1 lists the positions of 10 candidate 1.2 mm sources found in the MAMBO map, and Table 2 their flux densities. We fitted the sources in the map smoothed to $11''$ to Gaussians unconstrained in width, and in cases where the fitted width is smaller than the beam size, to constrained width Gaussians of $11''$ FWHM. The peak fluxes quoted in Table 2 are averages of Gauss fits in maps smoothed to $11''$ and $12''$, and to eliminate a base problem due to double beams surrounding the brighter sources, in a map truncated toward negative values at 0. The quoted uncertainties are quadratic sums of the dispersion in these three fits and the rms noise level at the position of the source in the $11''$ resolution map.

3.2. Identification of the mm sources

Due to the large MAMBO beam (FWHM $\sim 11''$), we often find several potential optical counterparts within the positional uncertainty. Higher resolution interferomet-

ric imaging would be needed for more unique identifications (*e.g.* Dannerbauer et al., 2002; Dunlop et al., 2003). Comparisons of positions derived from MAMBO maps and from the VLA or IRAM Plateau de Bure interferometer yield median offsets of $2-3''$ with a tail extending to $7-8''$ (Eales et al., 2003; Dannerbauer et al., 2004). To obtain more accurate positions, we can take advantage of the tight radio-to-far-infrared correlation in star-forming galaxies (*e.g.* Condon, 1992), which appears to hold out to high redshift (Garrett, 2002). Because the faint radio synchrotron emission traces the same region as the mm emission, we can use deep sub-arcsecond resolution 1.4 GHz VLA maps to pinpoint the dust emission to within $< 1''$ (*e.g.* Ivison et al., 2002).

The surface density of radio sources brighter than $30 \mu\text{Jy}$ is $\simeq 2.5 \text{ arcmin}^{-2}$ (Ivison et al., 2002), so we expect to find only 0.035 such sources within a radius of $4''$ from the MAMBO positions. Because $30 \mu\text{Jy}$ is at the 2σ noise level in our radio map, we expect to find 0.4 positive 2σ peaks within $4''$ from the nominal MAMBO positions. In an attempt to discriminate against noise peaks, we also checked for optical or near-IR counterparts for the radio sources. We consider an optical/near-IR source with a $> 2\sigma$ radio peak within the astrometric uncertainty of $0'.4$ as a likely counterpart to a MAMBO source, if it lies within $4''$ from the MAMBO position. In the following, we discuss the individual identifications of the 10 candidate MAMBO sources, and of an additional radio source in the field. Table 1 lists the mm, radio and optical positions, and Table 2 the photometric measurements.

M01 (Fig. 3): This is the brightest source in our MAMBO map. The identification is secure with a 4.4σ radio source coinciding with an $R=26.8$ source, which we used as the basis for SCUBA photometry. We have attempted deep VLT/FORS1 spectroscopy on this object (De Breuck et al. in preparation), but did not detect any emission, so the spectrum is not dominated by strong line emission from an AGN.

M02 (Fig. 3): This MAMBO source appears to consist of two components; an unconstrained Gaussian fit yields a size of $19'.7 \times 17'.0$. Within a radius of $5''$ from the MAMBO position, there are three 1.4 GHz sources with flux densities $S_{1.4\text{GHz}} > 45 \mu\text{Jy}$, i.e. at significance levels of $\sim 2\sigma$ (see Table 2), while we expect to find only one such source. This suggests a complex, merging structure of galaxies, as hinted by the diffuse R -band source coincident with the brightest of the three VLA sources, M02a (see Tables 1 and 2). We have used this position for the SCUBA photometry, but the relatively low S_{850}/S_{1200} ratio indicates that the SCUBA beam may have missed part of the flux, suggesting M02a is not the correct identification of the brightest 1.2 mm emission. Only interferometric (sub-)mm imaging could provide a better understanding of this interesting source.

M03 (Fig. 2): This 3.8σ MAMBO source lies $3'.2$ from the host galaxy of the powerful radio source (De Breuck et al., 1999), and is therefore most likely related. We used the K -band position to obtain MAMBO on-off observations

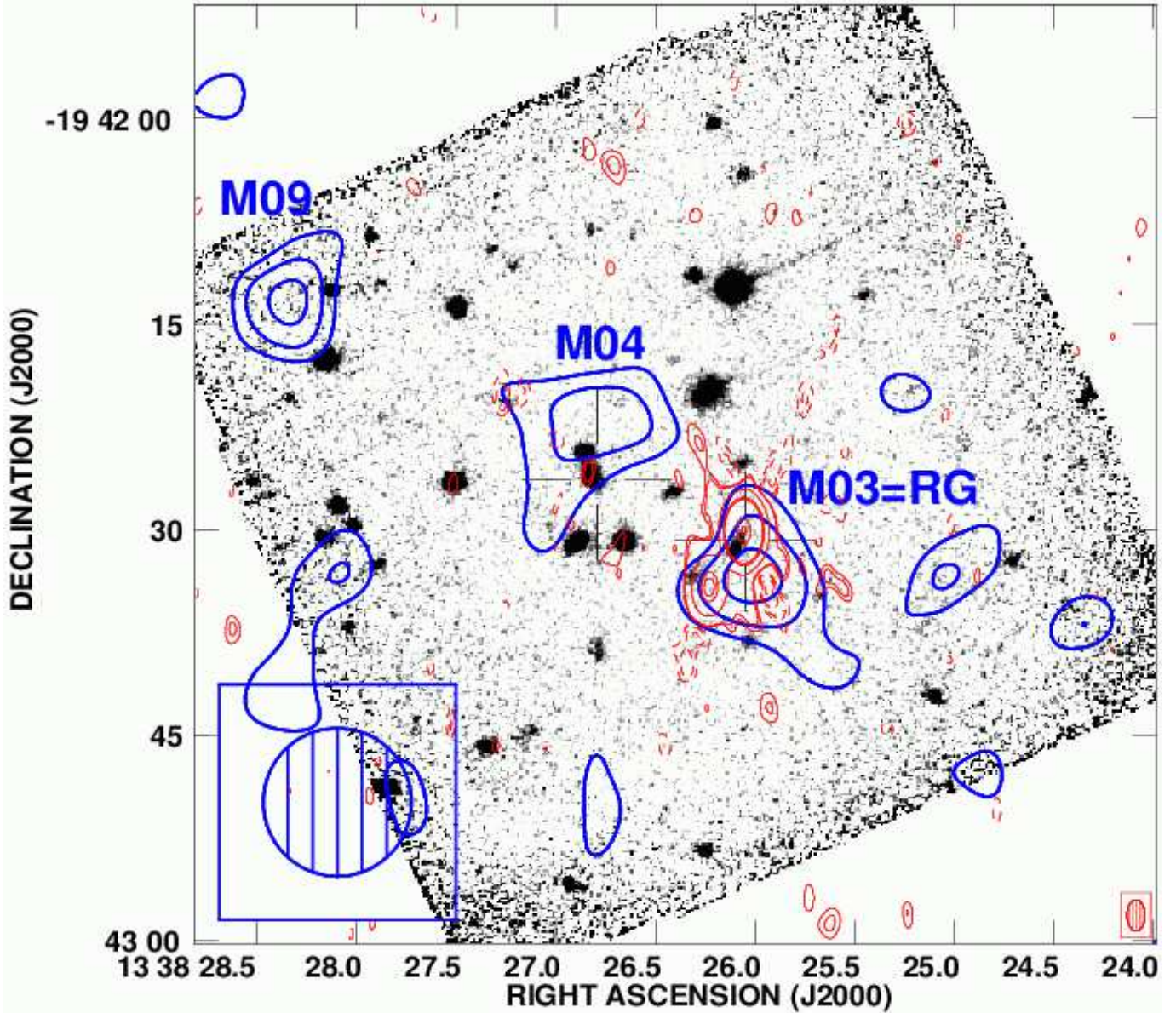


Fig. 2. Keck/NIRC K -band image (greyscales) with the MAMBO 1.2 mm signal-to-noise map (smoothed to $11''$) overlaid as thick/blue contours and the VLA 1.4 GHz map as thin/red contours. Contour levels for the MAMBO map are 2, 3 and 4σ , with σ the local rms noise level. Contour levels for the VLA map are -0.1275, -0.09, -0.063, -0.045, 0.045, 0.063, 0.72, 4.08, 5.775, 62.28 and 130.56 mJy/beam. The MAMBO and VLA beam sizes are indicated in the lower left and lower right corners, respectively. The open cross indicates the position of the optical/radio identification.

and SCUBA photometry, but both of these gave lower than expected flux densities (see Table 2), suggesting that the dust emission could be offset from the K -band position, as has been seen in the $z=3.79$ radio galaxy 4C 60.07 (Papadopoulos et al., 2000). In Table 2, we quote the S/N weighted average of our $S_{850\mu\text{m}}=3.1\pm1.8$ mJy measurement and the $S_{850\mu\text{m}}=6.9\pm1.1$ mJy of Reuland et al. (2004). We do not average the $450\mu\text{m}$ flux densities, as the Reuland et al. (2004) photometry was obtained under adverse atmospheric conditions leading to a nominal measurement of $S_{450\mu\text{m}} = -36.3 \pm 31.5$ mJy. Such discrepant $S_{850\mu\text{m}}$ flux densities between observations at different epochs have been noticed before for MG 2141+192

(Archibald et al., 2001; Reuland et al., 2004), and suggest submm variability. But, as Reuland et al. (2004) argue, the extended nature of the submm emission excludes this explanation, unless there is a significant contribution from non-thermal AGN emission. However, a power-law extrapolation from the total 8.2 GHz flux density (Pentericci et al., 2000) predicts a negligible AGN synchrotron contribution of only $30\mu\text{Jy}$ at 250 GHz, but given the unusually asymmetric morphology of the radio source (De Breuck et al., 1999), we cannot exclude the presence of a variable, flat spectrum radio core contributing to the submm flux densities, as has been seen in B2 0902+343

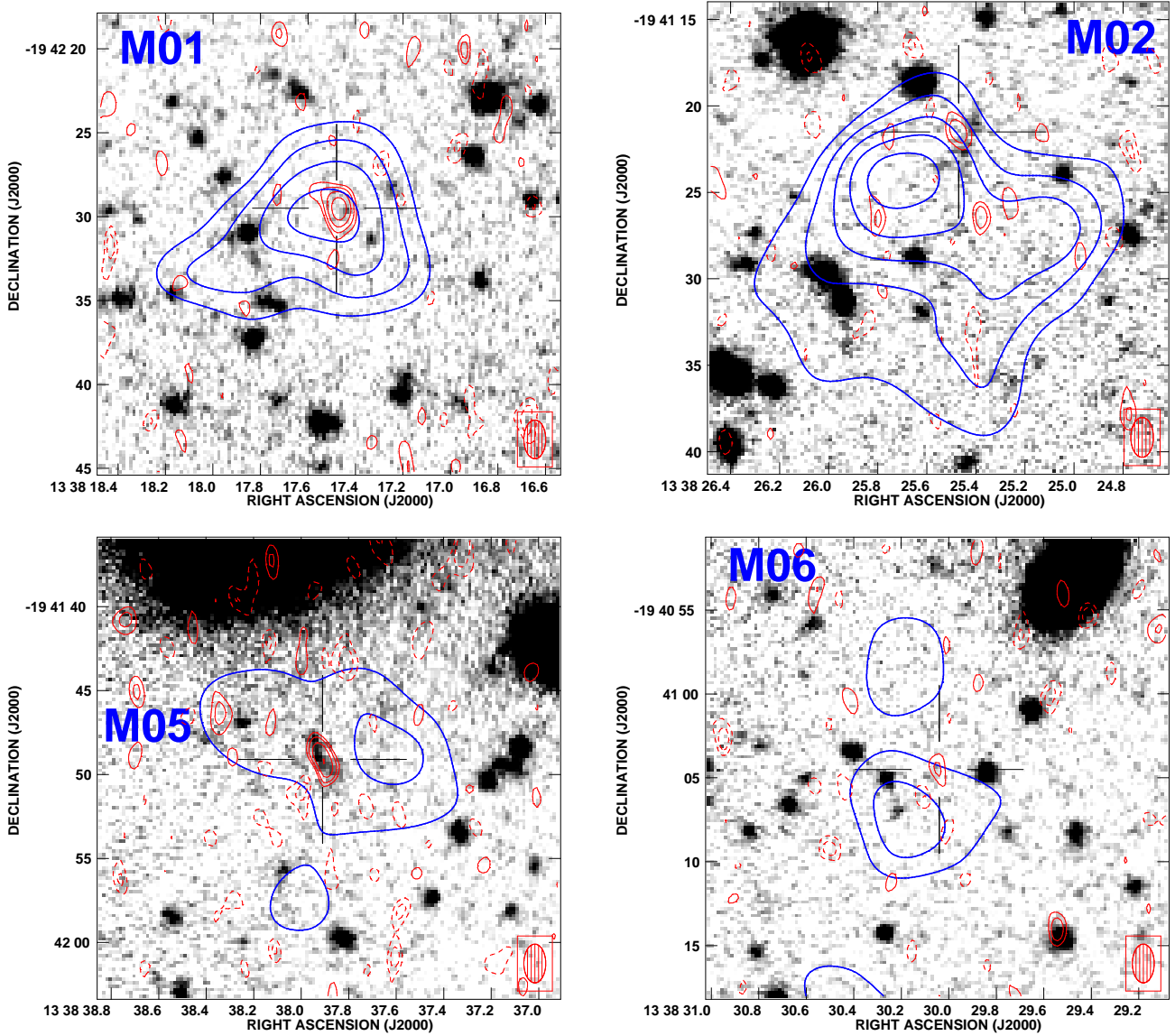


Fig. 3. VLT R -band image (greyscales) with the MAMBO 1.2 mm signal-to-noise map (smoothed to $11''$) overlaid as thick/blue contours and the VLA 1.4 GHz map as thin/red contours. Contour levels for the MAMBO map are 2, 3, 4, 5, 6 and 7σ , with σ the local rms noise level. Contour levels for the VLA map are -42, -30, 30, 42, 60 and $85 \mu\text{Jy/beam}$. The VLA beam size is indicated in the lower right corner. The open cross indicates the position of the optical/radio identification.

(Downes et al., 1996). High resolution imaging at frequencies of several tens of GHz would be needed to test this.

M04 (Fig. 2): This 4σ MAMBO source lies $3''.0$ from a faint radio source coincident with a very red galaxy with $R - K = 5.36 \pm 0.04$, which is a likely identification.

M05 (Fig. 3): We obtained SCUBA photometry of the extended radio and optical source, confirming the identification. This is the only source which has spatially extended 1.4 GHz emission; the close correspondence between the diffuse optical and radio morphologies strongly suggests the 1.4 GHz emission traces starburst rather than AGN emission. Deep VLT/FORS1 spectroscopy (De Breuck et al. in preparation) also revealed a faint featureless continuum, but no emission lines. An unconstrained

Gaussian fit to the MAMBO S/N map yields a size of $20''.8 \times 18''.0$, but the S/N of our detection is only 3.7 in a $11''$ smoothed map, so the detection of spatially extended emission is tentative at best.

M06 (Fig. 3): We obtained SCUBA photometry at the position of a very faint radio and optical identification, confirming the reality of this faint MAMBO source. Note that the apparent spatial extent of the MAMBO emission cannot be trusted because this source is only detected at the 3.4σ level.

M07 (Fig. 3): Although this is one of the brightest MAMBO sources, there is no obvious radio or optical identification. We have obtained SCUBA photometry of the radio/optical source at $\text{RA} = 13^{\text{h}}38^{\text{m}}30.22^{\text{s}}$,

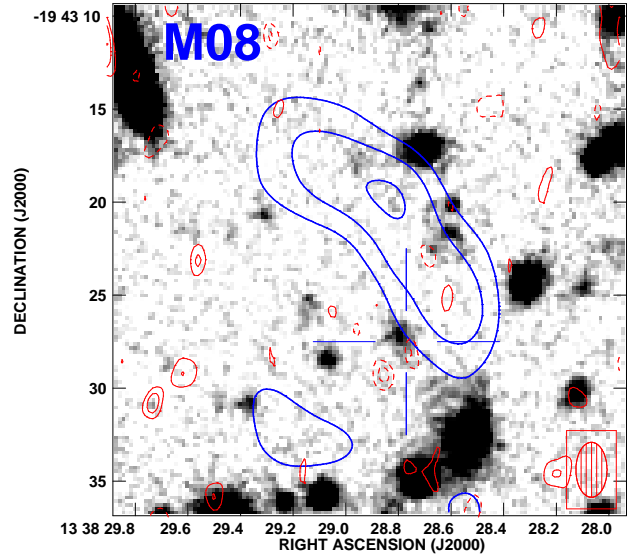
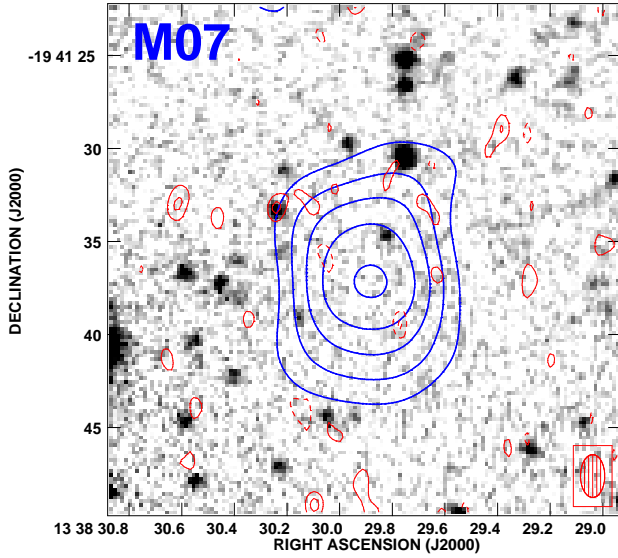


Fig. 3. , *continued*

DEC= $-19^{\circ}41'33''.06$, but obtained only a 1.5σ signal of $S_{850\mu\text{m}}=3.7\pm2.5$ mJy, while at the nominal MAMBO position, we obtain a slightly higher signal (see Table 2). We do not have a good candidate optical or radio counterpart for this MAMBO source.

M08 (Fig. 3): This faint MAMBO source lies $6''.7$ from an extremely red object (ERO) with $K=19.2\pm0.1$ and $R-K=6.1\pm0.15$. We have obtained deep FORS2/MXU spectroscopy of this ERO (Overzier et al., in preparation), detecting a faint red continuum and an emission line at 8120\AA , which we tentatively identify as $[\text{O II}] \lambda 3727$ at $z=1.18$. Note that from blank-field ERO surveys, the density of objects with $R-K>6$ and $K<19.2$ is 0.10 arcmin^{-2} (Daddi et al., 2000), so the chance of finding such an object within $6''.7$ is $P=0.4\%$. It is therefore possible that M08 is a dusty ERO (*e.g.* Cimatti et al., 1998; Dey et al., 1999; Smail et al., 2002b; Takata et al., 2003). However, because the ERO is not the closest possible identification, it is statistically not the most likely identification. Note that the apparent spatial extent of the MAMBO emission cannot be trusted because this source is only detected at the 4σ level. This may also indicate that this source has made it into our sample due to the confusion of two sources too close to be detected individually. Deeper mm/submm observations would be needed to verify this, and to determine if the dust emission is related to the ERO or not.

M09 (Fig. 2): We find no radio source within one MAMBO beamsize, and no clear optical/near-IR identifications.

M10 (Fig. 4): This MAMBO source falls just outside the VLT R -band image. It coincides with a strong 0.2 mJy radio source.

R1 (Fig. 1): This is a moderately bright radio source with a FR II (Fanaroff & Riley, 1974) morphology. We detect no 1.2 mm emission from this source.

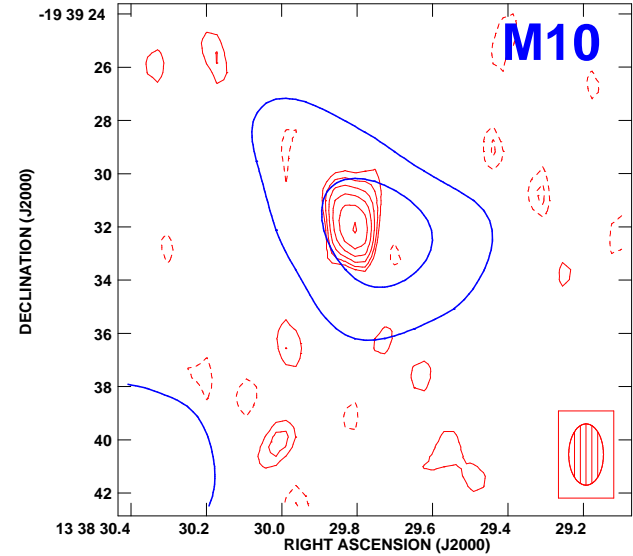


Fig. 4. M10: MAMBO 1.2 mm signal-to-noise map (thick/blue contours; smoothed to $11''$) and the VLA 1.4 GHz map (thin/red contours). Contour levels for the MAMBO map are 2 and 3σ , with σ the local rms noise level. Contour levels for the VLA map are $-42, -30, 30, 42, 60, 85, 120$ and $170 \mu\text{Jy/beam}$. The VLA beam size is indicated in the lower right corner. This source falls outside the VLT R -band image.

3.3. Extended 1.2mm emission

At least one (M02) of the three sources detected with $S/N>5$, and possibly the weaker source M05 appear to have significantly extended 1.2 mm emission. M02 appears to consist of two barely resolved components, though none of them have a clear candidate optical or radio identification. Spatially extended submm emission has been reported before in several HzRGs and at least two compan-

ion sources (Ivison et al., 2000; Stevens et al., 2003, Ivison et al., in prep.). This suggests that star formation in these objects occurs over scales of several tens of kpc.

A possible alternative explanation is that M02 (and maybe M05) could consist of multiple images by strong gravitational lensing by a foreground cluster (Kneib et al., 2004; Borys et al., 2004). However, we have not detected any gravitational arcs in the ACS/*HST* images (Miley et al., 2004) or in the VLT image (Fig. 1). We therefore consider it extremely unlikely that gravitational lensing can explain the spatial extent in the mm emission. A more detailed analysis of the lensing properties, including an analysis of a possible weak shear using the ACS image will be presented in a future paper (Overzier et al., in prep.).

3.4. Surface density

Although many of the MAMBO sources were detected at low S/N level, most of them appear to be real because because they have been confirmed with pointed sub-mm photometry, or because they have plausible counterparts at radio and/or optical wavelengths. We detect 10 sources brighter than 2.0 mJy (peak S/N>3, a level at which we should be close to being complete). Omitting M03, which corresponds to the pre-selected radio galaxy in the field, this corresponds to a surface density of 0.35 arcmin^{-2} (roughly 1% of the confusion limit). Note that this value is likely to be an overestimate because we consider sources down to the 3σ level, which may have lead to flux boosting (*e.g.* Eales et al., 2003). This effect raises intrinsically fainter sources above the detection threshold due to the addition of noise (instrumental and atmospheric) or due to confusion of sources too faint to be detected individually. The latter affect may be happening in M08 (Fig. 3). Eales et al. (2003) argue that for MAMBO surveys, the average boosting factor is 14%, which is slightly lower than for the SCUBA surveys, possibly due to the smaller MAMBO beam.

We now compare our surface density with the integrated 1.2 mm source counts from the MAMBO blank field surveys (Bertoldi et al., 2000). Using the 1.2 mm counts from Bertoldi (private communication) and Greve et al. (2004), our $S_{1.2\text{mm}}$ source density (without flux boosting correction) is roughly twice as high as expected from the random-field density. However, if we consider only the 3 sources with $S_{1.2\text{mm}} > 4 \text{ mJy}$, the source density is 0.12 arcmin^{-2} , three times higher than expected. Assuming a Poissonian distribution, this represents a 7σ overdensity. These bright sources are all detected with a local¹ S/N>5, so they will not be affected by flux boosting. This overdensity suggests that most of the brighter MAMBO sources and a few of the fainter ones may be related to the proto-cluster. Such statistical overdensities

Table 3. Photometric redshift estimates.

Source	z_{est} from $\alpha_{1.4\text{GHz}}^{250\text{GHz}}$	z_{est} from $S_{850\mu\text{m}}/S_{1200\mu\text{m}}$
M01	$2.2^{+1.7}_{-0.9}$	$6.8^{+\infty}_{-4.5}$
M02	$2.8^{+3.5}_{-1.3}$	$7.1^{+\infty}_{-4.9}$
M03 ^a	...	$7.1^{+11}_{-1.9}$
M04	$2.2^{+2.1}_{-1.1}$...
M05	$2.2^{+1.8}_{-1.0}$	$2.1^{+6.8}_{-2.1}$
M06	$2.2^{+4.1}_{-1.0}$	$2.4^{+14}_{-2.4}$
M07	>2.9	>4.2
M08 ^b	>2.3	...
M09	>2.3	...
M10	$1.5^{+1.1}_{-0.7}$...

^a Radio galaxy at $z=4.1$.

^b Possibly identified with a $z_{\text{spec}}=1.18$ ERO, see §3.2.

of SMGs are also seen in SCUBA maps of other HzRG fields (*e.g.* Stevens et al., 2003). In the next section, we use our radio, mm and submm photometry to constrain the redshifts of these MAMBO sources.

3.5. Photometric redshift estimates

We attempted very deep ($t_{\text{int}}=14\text{h}$) optical spectroscopy of M01 and M05, but did not detect features to determine the redshifts. None of the MAMBO sources show excess narrow-band emission in the $4.075 < z < 4.123$ coverage of the Ly α filter, and only M04 and M08 have K -band photometry, so we cannot use conventional optical photometric redshift techniques. As this is a common situation for submm galaxies, several redshift estimators have been developed based on the submm and radio data only.

Carilli & Yun (1999) proposed to use the radio-to-submm spectral index as a redshift estimator, which is based on the local radio-to-far-infrared correlation. Table 3 lists the redshift estimates calculated using the Carilli & Yun (2000) $\alpha_{1.4\text{GHz}}^{250\text{GHz}}$ models. The quoted uncertainties include both the 1σ measurement uncertainties in our photometry and the 1σ scatter in the models. The estimated redshifts are clearly lower than the $z=4.1$ of the radio galaxy, though $z=4.1$ is still within the 1σ uncertainties for most sources (except M10). However, a comparison with spectroscopic redshifts of SMGs indicates that the spectral-index redshifts tend to be systematically underestimated for $z_{\text{spec}} > 2$ objects (*e.g.* Clements et al., 2004). In fact, the Carilli & Yun (2000) models predict a spectral index $\alpha_{1.4\text{GHz}}^{250\text{GHz}}=1.00$ for $z=4.1$, so for the average $S_{1200}=3.3 \text{ mJy}$ in our maps, we expect to find a radio source with a flux density $S_{1.4\text{GHz}}=18\mu\text{Jy}$, well below the detection limit of our VLA map. However, Petric et al. (2003) report 1.4 GHz detections of $\sim 70\mu\text{Jy}$ in two $z > 5$ radio quiet quasars with S_{1200} flux densities of 0.9 and 5.5 mJy. A possible explanation for this higher than expected 1.4 GHz emission is that an optically undetected AGN contributes to the radio emission. Note that AGNs have been spectroscopically confirmed in two proto-clusters surrounding HzRGs (Le Fèvre et al., 1996; Pentericci et al., 2002), while Smail et al. (2003b) report

¹ Note that the uncertainties in Table 2 also include the fitting uncertainties (see §3.1), and are hence larger than the local rms.

the discovery of *Chandra* X-ray sources coincident with submm sources surrounding three HzRGs, suggesting the MAMBO sources surrounding TN J1338–1942 – if they are part of the protocluster – may well contain AGNs. Hence, a relatively bright radio detection of a MAMBO source does not exclude it as a potential member of the $z = 4.1$ protocluster.

Eales et al. (2003) have also predicted the redshift evolution of the $S_{850\mu\text{m}}/S_{1200\mu\text{m}}$ ratio, by fitting a two-temperature model to a sample of 104 galaxies from the IRAS bright galaxy survey (Dunne & Eales, 2001). We have used their median predicted value (Fig. 4 in the Eales et al., 2003, paper) to obtain an additional redshift estimate. Table 3 lists these estimates; the quoted uncertainties include the 1σ measurement uncertainties in the $S_{850\mu\text{m}}/S_{1200\mu\text{m}}$ ratios and the full spread in the model predictions. We find that, except for a $z > 2.2$ limit for M01 and M02, this ratio does not provide a useful constraint on the redshifts due to (i) the small difference in wavelength between the mm and submm points and (ii) the relatively low S/N of our detections.

In summary, while the radio, mm and submm photometry are generally consistent with $z=4.1$, the uncertainties from these redshift estimate techniques are far too large to provide proof that the sources are at the redshift of the radio galaxy. Better sampled SEDs, especially in the submm would be needed to constrain the redshifts with photometry only.

3.6. Statistical 1.2 mm and 1.4 GHz emission from the $\text{Ly}\alpha$ emitters and Mean Star Formation Rates

None of the 14 spectroscopically confirmed $\text{Ly}\alpha$ emitters within the $\sigma < 1.2$ mJy region (excluding the radio galaxy) is detected at $> 2\sigma$ in our 1.2 mm map. To test if there is a statistical signal in our non-detections, we have stacked the emission from these 14 positions, and find $\langle S_{1.2\text{mm}} \rangle = 0.25 \pm 0.24$ mJy. Using this 3σ upper limit, and assuming dust parameters $T_d = 33$ K and $\beta = 2.0$ used for LBGs (Baker et al., 2001), we derive $\langle L_{\text{FIR}} \rangle \lesssim 4.4 \times 10^{12} L_\odot$, implying a mean star formation rate $\langle \text{SFR}_{\text{FIR}} \rangle \lesssim 440 \text{ M}_\odot \text{yr}^{-1}$ (e.g. Omont et al., 2001).

Similarly, from our VLA map, we find $\langle S_{1.4\text{GHz}} \rangle = -0.2 \pm 2.9 \mu\text{Jy}$. Using the relation between the radio emission and star formation rate (Condon, 1992), we can use this 3σ upper limit of $8.7 \mu\text{Jy}$ on the 1.4 GHz emission to calculate an upper limit to the star formation rate (SFR) from the $\text{Ly}\alpha$ emitters. Assuming a radio spectral index $\alpha_{\text{radio}} = -0.8$, we derive $\langle \text{SFR}_{\text{radio}} \rangle < 265 \text{ M}_\odot \text{yr}^{-1}$.

The values should be compared with the SFR derived from the mean $\text{Ly}\alpha$ luminosity of the same 14 emitters (excluding the radio galaxy) $\langle L_{\text{Ly}\alpha} \rangle = 2.77 \times 10^{42} \text{ erg s}^{-1}$. Assuming a case B ratio $\text{Ly}\alpha/\text{H}\alpha = 10$, and using the Kennicutt, Tamblyn, & Congdon (1994) relation between SFR and $L_{\text{H}\alpha}$, we find $\langle \text{SFR}_{\text{Ly}\alpha} \rangle = 2.2 \text{ M}_\odot \text{yr}^{-1}$. Note that this value is likely to be an underestimate, as $\text{Ly}\alpha$ is often

quenched by dust emission, as illustrated by Kurk et al. (2004), who report $\text{Ly}\alpha/\text{H}\alpha$ ratios significantly lower than the case B value for a sample of $\text{Ly}\alpha$ and $\text{H}\alpha$ emitters surrounding the $z=2.16$ radio galaxy PKS 1138–262. However, it is obvious that the deep $\text{Ly}\alpha$ imaging probes much lower SFR than the MAMBO and VLA maps.

4. Discussion

Although we could not put strong constraints on the redshifts of the 9 MAMBO sources surrounding TN J1338–1942 using photometric redshift estimators or very deep VLT/FORS1 spectroscopy of two of them, the analysis of the source density and the photometric redshift estimates suggests half of the 9 MAMBO sources, and in particular the brightest ones, may well belong to the $z=4.1$ proto-cluster. To confirm (or refute) this requires alternative redshift determinations such as (i) deep near-IR spectroscopy, (ii) mid-IR spectroscopy with IRS/*Spitzer* using the PAH features, and (iii) mm spectroscopy using molecular CO lines.

Figure 1 shows that the nine MAMBO sources are not distributed uniformly around the radio galaxy, although the sensitivity of our MAMBO map radially decreases from the radio galaxy. The four brightest MAMBO sources (M01, M02, M07 and M05) are all north of the radio galaxy, while the densest area of $\text{Ly}\alpha$ emitters is located southeast of the radio galaxy (Venemans et al., 2002; Miley et al., 2004). This suggests that the centre of the proto-cluster is not necessarily to the southeast of the radio galaxy, as suggested by the distribution of $\text{Ly}\alpha$ emitters. None of the 14 spectroscopically confirmed $\text{Ly}\alpha$ emitters in the MAMBO field were detected at 1.2 mm or 1.4 GHz. Similarly, none of the MAMBO sources show excess $\text{Ly}\alpha$ emission (if they are within the $4.075 < z < 4.123$ coverage of the narrow-band $\text{Ly}\alpha$ filter). A possible explanation would be that their large amounts of dust, as traced by the 1.2 mm emission may have quenched the $\text{Ly}\alpha$ emission (e.g. Kunth et al., 1998), putting them below the narrow-band excess cutoff ($\text{EW}_{\text{rest}} > 15 \text{ \AA}$). This apparent absence of overlap between both populations shows the importance of using multiple wavelength techniques to obtain a more complete picture of the proto-cluster. Chapman et al. (2000) and Webb et al. (2003) also report a $< 20\%$ overlap between SMGs and LBGs, with a few notable exceptions (e.g. Chapman et al., 2002). However, Webb et al. (2003) do find a large cross-clustering correlation amplitude between both populations in the largest of their 3 fields. We do not detect enough MAMBO sources in the TN J1338–1942 field to perform such a cross-correlation analysis, but our detection of a statistical overdensity of MAMBO sources does suggest some relation to the confirmed overdensity of $\text{Ly}\alpha$ emitters (Venemans et al., 2002) and LBGs (Miley et al., 2004) in the same field.

The faintness of the $\text{Ly}\alpha$ in our objects also contrasts the published spectra of SMGs, which often show bright $\text{Ly}\alpha$ lines (Chapman et al., 2003). However, these

SMGs are on average at lower redshifts $\langle z \rangle \sim 2.4$ (Chapman et al., 2003), while our MAMBO sources are potential members of the $z=4.1$ proto-cluster. Although we only have K -band information for 3 sources, which are all relatively bright class-II ($I - K \lesssim 5$, $K \lesssim 21$) or class-I ($I - K \gtrsim 5$) sources (Ivison et al., 2000; Smail et al., 2002a), 3 of the 4 brightest MAMBO sources may well be very faint class-0 ($K \gtrsim 21$) sources which are much harder to obtain redshifts from (*e.g.* Dannerbauer et al., 2002; Frayer et al., 2004), either because they are more highly obscured, or because they are at higher redshifts. Our success in finding higher redshift objects may have been helped by the use of a longer selection wavelength (1.2 mm instead of 850 μm). Indeed, based on the low ratio of 850 μm to 1.2 mm flux, several authors argue that a significant fraction of mm galaxies may be at $z > 3$ (*e.g.* Eales et al., 2003; Aretxaga et al., 2003). Most MAMBO sources in the NTT deep field (Dannerbauer et al., 2002) are also class-0 sources, supporting the trend that 1.2 mm selected sources appear to be fainter (and hence maybe at higher redshift) than 850 μm selected sources.

The detection of X-ray emission in several bright submm sources within the proto-clusters surrounding three other HzRGs (Smail et al., 2003b) suggests that AGN may be present within those sources. Half of the spectra presented by Chapman et al. (2003) also show type-II AGN lines, but we failed to detect these in our very deep VLT spectroscopy of M01 and M05. Hence, we have no indication that AGN are present in our MAMBO sources, but their emission lines may well have been obscured (*e.g.* Reuland et al., 2003). Assuming the MAMBO sources are at $z=4.1$, and dust parameters $T_d = 50$ K and $\beta = 1.5$ (Benford et al., 1999), we derive $L_{\text{FIR}} \approx 2 \times 10^{13} L_{\odot} \times S_{1.2\text{mm}}/\text{mJy}$ in the range $4\text{--}12 \times 10^{13} L_{\odot}$, implying star formation rates of 4000 to 12000 $\text{M}_{\odot}\text{yr}^{-1}$, if the dust is entirely heated by star formation (*e.g.* Omont et al., 2001; De Breuck et al., 2003). For M08, which is possibly at $z=1.18$, we derive $L_{\text{FIR}} \approx 1.6 \times 10^{13} L_{\odot}$ and a star formation rate of 1600 $\text{M}_{\odot}\text{yr}^{-1}$. Such high star formation rates have been reported for HzRGs (Archibald et al., 2001; Reuland et al., 2004), but our MAMBO map indicates that they may also occur out to distances as far as 2 Mpc from the central radio galaxy. If the MAMBO sources are really at $z=4.1$, this would suggest that these proto-clusters have multiple, possibly aligned (Pentericci et al., 2002) concentrations. However, the VLT narrow-band $\text{Ly}\alpha$ image shows that none of the mm sources seen in the TN J1338–1942 proto-cluster have huge $\text{Ly}\alpha$ haloes, like those seen around the central HzRG (*e.g.* Venemans et al., 2002; Reuland et al., 2003). The HzRG therefore appears the best candidates to evolve into the present-day giant elliptical.

5. Conclusions

We summarize the results from our multi-wavelength observations of the $z=4.1$ proto-cluster surrounding TN J1338–1942 as follows:

- We detect 10 candidate mm sources with peak fluxes having $S/N > 3$ in our MAMBO map. Of these, at least eight sources with $S_{1.2\text{mm}} > 1.3$ mJy have possible radio and/or optical/near-IR counterparts, and 5 are confirmed at $S/N > 4$ with pointed SCUBA submm photometry. Three sources have $S_{1.2\text{mm}} > 4.0$ mJy, while comparing with source counts from blank field surveys, we expect to find only 1 such source in the unassociated field population.

- The radio-to-submm and mm-submm photometric redshift estimates do not provide strong constraints on the possible redshifts of the MAMBO sources, although for 9 of the 10 sources, they are consistent with $z=4.1$ within the uncertainties.

- One of the faint MAMBO sources is possibly related to an ERO with $R - K = 6.1$, which has a likely spectroscopic redshift of $z=1.18$, implying a star formation rate up to 1600 $\text{M}_{\odot}\text{yr}^{-1}$.

- None of the 14 spectroscopically confirmed $\text{Ly}\alpha$ emitters show detectable millimetre emission, and supposing they are at $z=4.1$, none of the 1.2 mm sources show an excess $\text{Ly}\alpha$ emission, indicating no apparent overlap between both populations.

- The mean star formation rate of the 14 spectroscopically confirmed $\text{Ly}\alpha$ emitters, as derived from the deep $\text{Ly}\alpha$ imaging is two orders of magnitudes lower than the upper limits derived from the stacked VLA and MAMBO maps, illustrating that the radio and mm maps probe much more actively star-forming galaxies.

Our multi-wavelength observations of this $z=4.1$ proto-cluster suggest that the $\text{Ly}\alpha$ excess technique does not detect the massive starburst companions within 2 Mpc. Their high SFR could be triggered by interactions between different proto-cluster members, as indicated by the diffuse nature of the optical identifications of M05 and M02.

Acknowledgements. We thank Thomas Greve for useful discussions. IRAM is supported by INSU/CNRS (France), MPG (Germany) and IGN (Spain). The National Radio Astronomy Observatory (NRAO) is operated by Associated Universities, Inc., under a cooperative agreement with the National Science Foundation. The JCMT is operated by JAC, Hilo, on behalf of the parent organizations of the Particle Physics and Astronomy Research Council in the UK, the National Research Council in Canada, and the Scientific Research Organization of the Netherlands. This work was supported by a Marie Curie Fellowship of the European Community programme 'Improving Human Research Potential and the Socio-Economic Knowledge Base' under contract number HPMF-CT-2000-00721, and by the European RTN programme "The Physics of the Intergalactic Medium". The work by MR and WvB at IGPP/LLNL was performed under the auspices of the U.S. Department of Energy, National Nuclear Security Administration by the University of California, Lawrence Livermore National Laboratory under contract No. W-7405-Eng-48. This work was carried out in the context of EARA, the European Association for Research in Astronomy.

References

- Archibald, E., Dunlop, J., Hughes, D., Rawlings, S., Eales, S., & Ivison, R. 2001, *MNRAS*, 323, 417
- Aretxaga, I., Hughes, D., Chapin, E., Gaztañaga, E., Dunlop, J., & Ivison, R. 2003, *MNRAS*, 342, 759
- Baker, A., Lutz, D., Genzel, R., Tacconi, L., & Lehnert, M. 2001, *A&A*, 372, L37
- Benford, D., Cox, P., Omont, A., Phillips, T., & McMahon, R. 1999, *ApJ*, 518, L65
- Bertoldi, F., et al. 2000, *A&A*, 360, 92
- Best, P. 2000, *MNRAS*, 317, 720
- Best, P. 2002, *MNRAS*, 336, 1293
- Best, P., Lehnert, M., Miley, G., & Röttgering, H. 2003, *MNRAS*, 343, 1
- Borys, C., et al. 2004, *MNRAS*, in press, astro-ph/0404473
- Cardelli, J., Clayton, G., & Mathis, J. 1989, *ApJ*, 345, 245
- Carilli, C. & Yun, M.-S. 1999, *ApJ*, 513, L13
- Carilli, C. & Yun, M.-S. 2000, *ApJ*, 530, L618
- Chapman, S., et al. 2000, *MNRAS*, 319, 318
- Chapman, S., et al. 2001, *ApJ*, 548, L17
- Chapman, S., Shapley, A., Steidel, C., & Windhorst, R. 2002, *ApJ*, 572, L1
- Chapman, S., Blain, A., Ivison, R., & Smail, I. 2003, *Nature*, 422, 695
- Cimatti, A., Andreani, P., Röttgering, H., & Tilanus, R. 1998, *Nature*, 392, 895
- Clements, D., et al. 2004, *MNRAS*, in press, astro-ph/0312269
- Condon, J. 1992, *ARA&A*, 30, 575
- Daddi, E., et al. 2000, *A&A*, 361, 535
- Daddi, E., et al. 2003, *ApJ*, 588, 50
- Dannerbauer, H., et al. 2002, *ApJ*, 573, 473
- Dannerbauer, H., et al. 2004, *ApJ*, 606, 664
- De Breuck, C., van Breugel, W., Minniti, D., Miley, G., Röttgering, H., & Carilli, C. 1999, *A&A*, 352, L51
- De Breuck, C., van Breugel, W., Stanford, S. A., Röttgering, H., Miley, G., & Stern, D. 2002, *AJ*, 123, 637
- De Breuck, C., et al. 2003, *A&A*, 401, 911
- Deutsch, E. 1999, *AJ*, 118, 1882
- Dey, A., Graham, J., Ivison, R., Smail, I., Wright, G., & Liu, M. 1999, *ApJ*, 519, 610
- Downes, D., Solomon, P., Sanders, D., & Evans, A. 1996, *A&A*, 313, 91
- Dunlop, J., et al. 2003, *MNRAS*, submitted, astro-ph/0205480
- Dunne, L. & Eales, S. 2001, *MNRAS*, 327, 697
- Eales, S., Bertoldi, F., Ivison, R., Carilli, C., Dunne, L., & Owen, F. 2003, *MNRAS*, 344, 169
- Fanaroff, B. & Riley, J. 1974, *MNRAS*, 167, 31P
- Frayser, D., Reddy, N., Armus, L., Blain, A., Scoville, N., & Smail, I. 2004, *AJ*, 127, 728
- Garrett, M. 2002, *A&A*, 384, L19
- Greve, T., Ivison, R., Bertoldi, F., Stevens, J., Dunlop, J., & Lutz, D. 2004, *MNRAS*, submitted
- Hill, G. & Lilly, S. 1991, *ApJ*, 367, 1
- Holland, W., et al. 1999, *MNRAS*, 303, 659
- Hu, E., Cowie, L., & McMahon, R. 1998, *ApJ*, 502, L99
- Hu, E., et al. 2002, *ApJ*, 568, L75
- Ivison, R., Dunlop, J., Smail, I., Dey, A., Liu, M., & Graham, J. 2000, *ApJ*, 542, 27
- Ivison, R., et al. 2002, *MNRAS*, 337, 1
- Jenness, T., SURF-SCUBA user reduction facility, Starlink User Note 216.1
- Kauffmann, G., Colberg, J., Diaferio, A., & White, S. 1999, *MNRAS*, 307, 529
- Kennicutt, R., Tamblyn, P., & Congdon, C. 1994, *ApJ*, 435, 22
- Kneib, J.-P., et al. 2004, *MNRAS*, 349, 1211
- Kodaira, K., et al. 2003, *PASJ*, 55, L17
- Kreysa, E., et al. 1998, *Proc. SPIE*, 3357, 319
- Kunth, D., Mas-Hesse, J., Terlevich, E., Terlevich, R., Lequeux, J., & Fall, S. 1998, *A&A*, 334, 11
- Kurk, J., et al. 2000, *A&A*, 358, L1
- Kurk, J., Pentericci, L., Röttgering, H., & Miley, G. 2004, *A&A*, in press
- Le Fèvre, O., Deltorn, J., Crampton, D., & Dickinson, M. 1996, *ApJ*, 471, L11
- Miley, G., et al. 2004, *Nature*, 427, 47
- Napier, P., Thompson, A., & Ekers, R. 1983, *Proc. IEEE*, 71, 1295
- Omont, A., Cox, P., Bertoldi, F., McMahon, R., Carilli, C., & Isaak, K. 2001, *A&A*, 374, 371
- Papadopoulos, P., et al. 2000, *ApJ*, 528, 626
- Pentericci, L., Van Reeve, W., Carilli, C., Röttgering, H., & Miley, G. 2000, *A&AS*, 145, 121
- Pentericci, L., et al. 2000, *A&A*, 361, L25
- Pentericci, L., Kurk, J., Carilli, C., Harris, D., Miley, G., & Röttgering, H. 2002, *A&A*, 396, 109
- Petric, A., Carilli, C., Bertoldi, F., Fan, X., Cox, P., Strauss, M., Omont, A., & Schneider, D. 2003, *AJ*, 126, 15
- Reuland, M., et al. 2003, *ApJ*, 592, 755
- Reuland, M., van Breugel, W., Röttgering, H., & De Breuck, C. 2004, *MNRAS*, submitted
- Rhoads, J., et al. 2003, *AJ*, 125, 1006
- Rocca-Volmerange, B., Le Borgne, D., De Breuck, C., Fioc, M., & Moy, E. 2004, *A&A*, 415, 931
- Schlegel, D., Finkbeiner, D., Davis, M. 1998, *ApJ*, 500, 525
- Shimasaku, K., et al. 2003, *ApJ*, 586, L111
- Smail, I., Owen, F., Morrison, G., Keel, W., Ivison, R., & Ledlow, M. 2002b, *ApJ*, 581, 844
- Smail, I., Ivison, R., Blain, A., & Kneib, J.-P. 2002a, *MNRAS*, 331, 495
- Smail, I., et al. 2003a, *ApJ*, 583, 551
- Smail, I., Scharf, C., Ivison, R., Stevens, J., Bower, R., & Dunlop, J. 2003b, *ApJ*, 599, 86
- Spergel, D., et al. 2003, *ApJS*, 148, 175
- Steidel, C., Adelberger, K., Dickinson, M., Giavalisco, M., Pettini, M., & Kellogg, M. 1998, *ApJ*, 492, 428
- Steidel, C., Adelberger, K., Shapley, A., Pettini, M., Dickinson, M., & Giavalisco, M. 2000, *ApJ*, 532, 170
- Stevens, J., et al. 2003, *Nature*, 425, 264

- Stevens, J., Page, M., Ivison, R., Smail, I. & Carrera, F.
2004, ApJ, 604, L17
- Takata, T. et al. 2003, PASJ, 55, 789
- Taylor, G., Carilli, C., & Perley, R. 1999, ASP
Conf. Ser. 180: Synthesis Imaging in Radio Astronomy
II
- Tonry, J. et al. 2003, ApJ, 594, 1
- van Breugel, W., et al. 2003, Proc. SPIE, 4834, 24
- van Dokkum, P., Franx, M., Fabricant, D., Kelson, D., &
Illingworth, G. 1999, ApJ, 520, L95
- Venemans, B., et al. 2002, ApJ, 569, L11
- Venemans, B., Miley, G., Kurk, J., Röttgering, H., &
Pentericci, L. 2003, The Messenger, 111, 36
- Webb, T., et al. 2003, ApJ, 582, 6
- Zylka, R., The MOPSI Cookbook, www.mpifr-bonn.mpg.de/staff/bertoldi/mambo/